

Upper mantle velocity-temperature conversion and composition determined from seismic refraction and heat flow

H.K.C. Perry, C Jaupart, J.-C Mareschal, N. M. Shapiro

▶ **To cite this version:**

H.K.C. Perry, C Jaupart, J.-C Mareschal, N. M. Shapiro. Upper mantle velocity-temperature conversion and composition determined from seismic refraction and heat flow. Journal of Geophysical Research : Solid Earth, 2006, 111 (7), 10.1029/2005JB003921 . insu-01270068

HAL Id: insu-01270068

https://insu.hal.science/insu-01270068

Submitted on 12 Feb 2016

HAL is a multi-disciplinary open access archive for the deposit and dissemination of scientific research documents, whether they are published or not. The documents may come from teaching and research institutions in France or abroad, or from public or private research centers.

L'archive ouverte pluridisciplinaire **HAL**, est destinée au dépôt et à la diffusion de documents scientifiques de niveau recherche, publiés ou non, émanant des établissements d'enseignement et de recherche français ou étrangers, des laboratoires publics ou privés.

Upper mantle velocity-temperature conversion and composition determined from seismic refraction and heat flow

H. K. C. Perry,[1] C. Jaupart,[1] J.-C. Mareschal,[2] and N. M. Shapiro[3]

Received 1 July 2005; revised 22 December 2005; accepted 22 March 2006; published 4 July 2006.

[1] We compile upper mantle P_n velocities from seismic refraction/wide-angle reflection surveys in the southern Superior Province of the Canadian Shield and compare them with temperatures at the Moho deduced from heat flow data. Calculated Moho temperatures and P_n velocities correlate well, showing that in this area, P_n depends primarily on temperature. The obtained values of $\partial V(P_n)/\partial T$ depend weakly on the assumed value of Moho heat flow and are on the order of $-6.0 \times 10^{-4} \pm 10\%$ km s^{-1} K^{-1}, within the range of temperature derivatives obtained in laboratory studies of ultramafic rocks. Comparison between observed P_n velocities and predicted values for several mineralogical models at Moho temperatures allows constraints on both the Moho heat flow and the shallow mantle composition. For all Moho heat flows, undepleted (clinopyroxene-rich) mantle compositions do not allow a good fit to the data. For depleted mantle compositions, temperatures consistent with the observed P_n velocities correspond to values of Moho heat flow larger than 12 mW m^{-2}. For our preferred Moho heat flow of 15 mW m^{-2}, the best fit mantle composition is slightly less depleted than models for average Archean subcontinental lithospheric mantle. This may be due to rejuvenation by melt-related metasomatism during the Keweenawan rifting event. The similarity in $P_n - T$ conversion factors estimated from this empirical large-scale geophysical study and those from laboratory data provides confidence in the absolute temperature values deduced from heat flow measurements and seismic studies.

Citation: Perry, H. K. C., C. Jaupart, J.-C. Mareschal, and N. M. Shapiro (2006), Upper mantle velocity-temperature conversion and composition determined from seismic refraction and heat flow, *J. Geophys. Res.*, *111*, B07301, doi:10.1029/2005JB003921.

1. Introduction

[2] A large part of the high-resolution information about the Earth's interior is provided by seismology, usually through tomographic inversions of large traveltime data sets. This information is often presented in the form of three-dimensional distributions of seismic wave speeds which may be converted into physical parameters such as temperature and density. Variations of seismic wave speed with temperature and pressure [e.g., *Sobolev et al.*, 1996; *Goes et al.*, 2000] have been measured in the laboratory on individual mantle minerals as well as on a few rock samples. For a local study, therefore, interpretation requires a model of mantle composition inferred from geological observations and geochemical constraints [e.g., *McDonough and Rudnick*, 1998; *Griffin et al.*, 2003]. Calculating temperature from seismic wave speed is affected by significant uncertainties due to the starting compositional model and to the effects of anelasticity and fluids on physical properties. Therefore it is important, where possible, to calibrate this conversion with direct observations within the Earth. For this goal, we combined two data sets that provide the most direct estimates of seismic wave speeds and temperature in the uppermost mantle beneath the Superior Province of the Canadian Shield. In this study, we compare observed upper mantle compressional wave velocities at Moho depth (P_n) with those predicted from laboratory data and temperatures estimated from downward extrapolation of heat flow measurements.

[3] We chose P_n velocities because they are determined locally and are not affected by spatial smoothing inherent to tomographic analyses. P_n velocities are deduced from seismic refraction data and are characteristic of the refracted wave that propagates through the mantle just below the Moho discontinuity. These body waves sample the average wave speed over a few kilometers at the wavefront. Spatial resolution along the seismic line depends on the receiver spacing and on local heterogeneity, and is typically ~100 km [*Musacchio et al.*, 2004]. In contrast, tomographic studies are based on surface wave or teleseismic data and rely on inversions over a block structure. Resolution in the upper mantle is seldom better than 100 × 100 km along the

[1] Laboratoire de Dynamique des Systèmes Géologiques, Institut de Physique du Globe de Paris, Paris, France.
[2] Centre de Recherche en Geochimie et en Geodynamique, Université du Québec à Montréal, Montréal, Québec, Canada.
[3] Laboratoire de Sismologie, Institut de Physique du Globe de Paris, Paris, France.

Copyright 2006 by the American Geophysical Union.
0148-0227/06/2005JB003921$09.00

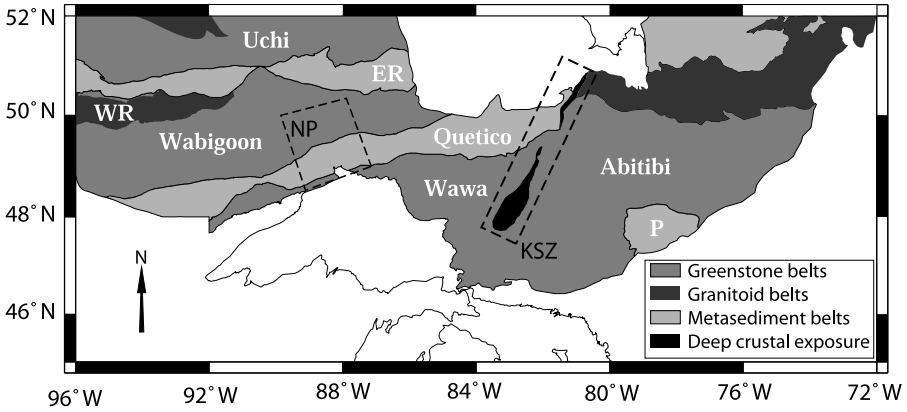


Figure 1. Geological map of the southern Superior Province. The Kapuskasing structural zone is the NE trending lens-like feature extending from 48°N to 50°N (KSZ in the dashed rectangle). The Keewenawan rift follows Lake Superior and extends to the north in the region of Lake Nipigon (NP in the dashed box). The Uchi, English River (ER), Winnipeg River (WR), Wabigoon, Quetico, Wawa, Abitibi, and Pontiac (P) subprovinces are shown.

horizontal and 20 km along the vertical [*Shapiro and Ritzwoller*, 2004]. *Herrin and Taggert* [1962] and *Herrin* [1969] have established the regional character of variations of traveltime anomalies and P_n velocities in the United States. These variations have been linked to temperature anomalies [*Horai and Simmons*, 1968], density anomalies [*Pakiser and Steinhart*, 1964; *Warren and Healy*, 1973], and compositional differences in the uppermost mantle [*Chung*, 1977]. *Pakiser* [1963] noted that crustal thickness and P_n velocity were related to one another and used an isostatic balance to derive a relationship between P_n velocity and upper mantle density. He realized, however, that seismic velocity is more sensitive to temperature than composition. *Black and Braile* [1982] examined the relationship between mean P_n velocity and heat flow for the main physiographic provinces of North America. Using a rough thermal model, they obtained an empirical temperature derivative for P_n velocity in approximate agreement with laboratory measurements. Recently, a slightly modified Black and Braile relationship has been proposed for the northern Canadian Cordillera [*Lewis et al.*, 2003].

[4] Rather than seeking correlations between bulk geophysical variables such as crustal thickness, heat flow and P_n velocities, we are interested in temperature variations in the crust and shallow mantle as well as in the lithospheric mantle composition. Heat flow data allow prediction of temperature and, through a mineralogical model, of P_n velocity. These calculations depend on the amount of radioelements in the crust as well as on the shallow mantle composition. Comparing predicted and observed P_n velocities therefore yields constraints on both variables.

[5] The Canadian multidisciplinary geoscience program LITHOPROBE has made available vast seismic data sets that sample all of the Archean and Proterozoic provinces of the Canadian Shield [*Clowes et al.*, 1999]. A summary of crustal structure at 5° × 5° resolution over the entire Canadian Shield based on LITHOPROBE data was provided by *Perry et al.* [2002]. At the scale of a whole continent juxtaposing provinces of different ages and geological histories, the relationship between mantle seismic velocity and temperature is likely to be contaminated by differences in mantle composition. One of the regions best sampled by seismic refraction/wide-angle reflection data is the southern part of the Archean Superior Province of the Canadian Shield. Because this region has also been extensively sampled by heat flow measurements, it provides an ideal area to study the relationship between mantle seismic velocity and temperature. We have thus compiled all available P_n velocity data and determined upper mantle temperatures from heat flow data in the Superior Province. Because of the dense sampling in this region, the data were interpolated on a 2° × 2° grid. On this scale, we show correlations between P_n and upper mantle temperature for 25 cells where both heat flow and seismic refraction data exist. The velocity-temperature conversion inferred from this large-scale geophysical study is in close agreement with laboratory measurements. We shall show that, in the study area, the Moho temperature varies by about 300 K, implying significant changes of seismic P wave velocity (3%). Such temperature variations are due solely to differences in crustal heat production and are systematic on scales as large as 300–500 km, reflecting the geological structure of the province.

2. Seismic and Heat Flow Data in the Superior Province

2.1. P_n Velocities

[6] The main geological units of the southern Superior Province are shown in Figure 1. The province is made of several east-west trending belts, alternating between volcano-plutonic belts (Uchi, Wabigoon, Wawa, and Abitibi) and metasedimentary belts (English River and Quetico). A gross trend of decreasing age (3.0–2.6 Ga) from north to south reflects the progressive accretion of these belts onto the craton. The region was subjected to major perturbations at 1.9 Ga, which saw the Kapuskasing Uplift, and at 1.1 Ga when the Keweenawan Rift led to the emplacement of large volumes of basalt. P_n velocities and crustal thickness were taken from the LITH5.0 model [*Perry et al.*, 2002] and a recent study of the western part of the province [*Musacchio et al.*, 2004]. The resolution of the data presented here is

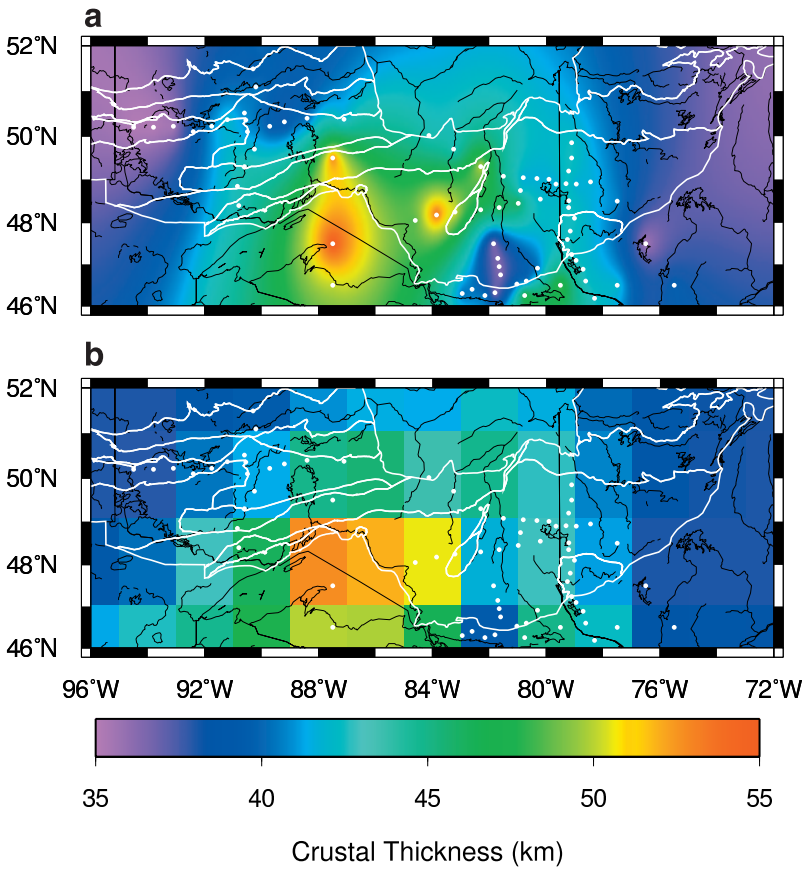


Figure 2. Crustal thickness as given by the LITH5.0 crustal model [*Perry et al.*, 2002] modified to include new western Superior data from *Musacchio et al.* [2004]. (a) Smoothed to 0.05° × 0.05° and (b) true 2° × 2° resolution. The white dots show the location of the seismic refraction/wide-angle reflection lines. The white lines mark the boundaries between the various subprovinces of the Superior Province that are defined in Figure 1.

2° × 2°. Crustal thickness is shown in Figure 2. The thickest crust reaches ~55 km in the Mid-Continent Rift (Keweenawan) beneath Lake Superior. The distribution of P_n velocity is shown in Figure 3.

[7] A correlation between P_n velocity and crustal thickness is apparent through comparison of Figures 2 and 3. Elastic properties depend on pressure and hence variations of Moho depth imply variations of seismic wave speed at constant temperature. From laboratory experiments, $(\partial V/\partial P)_T \approx 0.15$ km s^{-1} GPa^{-1} [*Christensen*, 1974; *Manghnani et al.*, 1974]. For an average crustal density of 2800 kg m^{-3}, the pressure correction is about 4.2×10^{-3} km s^{-1} km^{-1}. In the present context, however, such a correction may be neglected and the correlation between P_n velocity and crustal thickness may be attributed solely to temperature. Interpretation requires heat flow data and an accurate crustal model. For example, the thick crust near the Mid-Continent Rift does not necessarily imply elevated Moho temperatures because the volcanic rocks of the rift have low heat production and surface heat flow is low [*Perry et al.*, 2004].

2.2. Seismic Anisotropy

[8] For the purpose of comparing P_n velocities and upper mantle temperatures, one must sometimes account for anisotropy in the continental upper mantle [*Vinnik et al.*, 1992; *Silver*, 1996; *Debayle and Kennett*, 2000]. In the southwestern part of the Superior Province, the fast polarization axis for *S* waves is directed east-west [*Silver and Chan*, 1991; *Kay et al.*, 1999]. In many cases, it may be difficult to separate the effects of true seismic anisotropy (i.e., due to preferred orientation of minerals) from those of mantle heterogeneity and complex Moho topography [*Silver and Chan*, 1991]. Here, however, such separation is allowed by two intersecting seismic lines west of the Nipigon Embayment [*Musacchio et al.*, 2004]. In this area, there is no detectable seismic anisotropy in mantle material just below the Moho, i.e., in the P_n velocity. *P* wave anisotropy of ~6% is determined in only a shallow 50–75 km thick layer lying in the upper mantle 10–15 km below crust of normal thickness [*Musacchio et al.*, 2004]. This layer is interpreted as remnant oceanic lithosphere and does not affect the local P_n velocity determination.

2.3. Heat Flow and Heat Production

[9] Heat flow and heat production data used in this study come from a recent compilation including new measurements for the Superior Province by *Perry et al.* [2006], where a description of the methods used may be found. The mean heat flow for the Superior Province is 41.2 ± 7.3 mW m^{-2} based on 64 land heat flow determinations. Errors on individual heat flow determinations are estimated

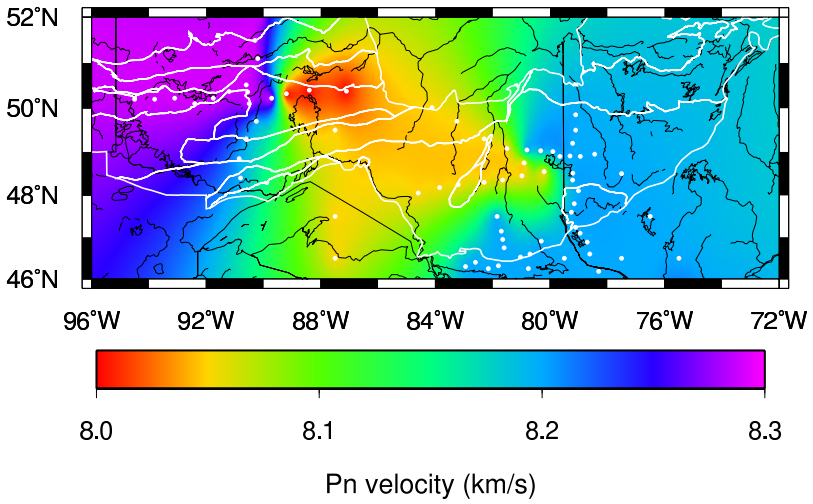


Figure 3. P_n velocity as defined in the LITH5.0 crustal model [*Perry et al.*, 2002] with the western Superior data of *Musacchio et al.* [2004] added. Results are smoothed to 0.05° × 0.05°. Red represents slow P_n wave speed, and blue represents fast wave speed. The white dots show the location of the seismic refraction/wide-angle reflection lines. The white lines mark the subprovince geological boundaries of the Superior Province.

to be <2 mW m^{-2}. These heat flow measurements sample the southern part of the Superior Province including the Uchi, English River, Wabigoon, Quetico, Wawa, and Abitibi belts (Figure 4). The study area includes Lake Superior where a marine heat flow survey was made [*Hart et al.*, 1994]. These measurements are not as accurate at those made in deep boreholes on land, however they show a consistent pattern with the land heat flow data.

[10] For given values of the surface heat flow, temperatures in the crust and at the Moho discontinuity depend on the amount and vertical distribution of heat producing elements in the crust. Crustal models with a uniform distribution of radioelements give higher Moho temperatures than models in which radiogenic heat production is concentrated in the upper crust. The distribution of radiogenic heat sources in the crust can be estimated from geological and geophysical evidence in combination with values of heat flow at the surface and at the Moho [*Perry et al.*, 2006]. In this region, strong constraints on crustal structure are provided by a deep crustal section exposed at the Kapuskasing site between the Wawa and Abitibi subprovinces.

3. Moho Temperature

3.1. Distribution of Heat Production

[11] On the scale of the Superior Province, one may assume that the Moho heat flow is constant. Evidence and

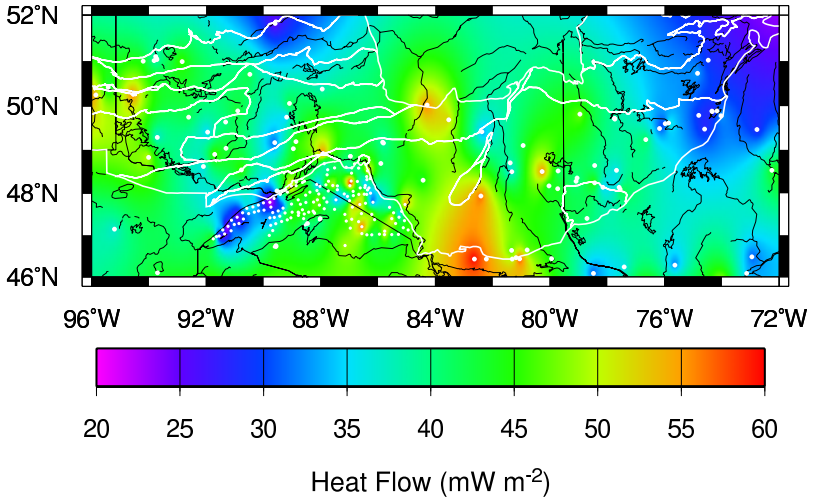


Figure 4. Heat flow in the Superior Province. The large white circles show the land heat flow measurement sites. Results are smoothed to 0.05° × 0.05°. The small white circles are lake heat flow sites from *Hart et al.* [1994]. The white lines mark the subprovince geological boundaries of the Superior Province.

arguments which support this have been developed at length by *Jaupart et al.* [1998] and *Mareschal and Jaupart* [2004], and we only recapitulate the main points. Variations of Moho heat flow, if they exist, would be due to changes of heat supply at the base of the lithosphere which are smoothed out by horizontal heat diffusion. Through ~250-km-thick Archean lithosphere, wavelengths less than 1000 km are strongly attenuated and all wavelengths shorter than 500 km are eliminated. This is supported by analysis of heat flow and heat production data. Heat flow variations can entirely be accounted for by changes of crustal heat production. Variations in Moho heat flow are less than the uncertainty on the heat flow estimates (2 mW m^{-2}) and cannot be detected.

[12] Using the systematics of heat flow and heat production distributions together with geological and geophysical constraints on the crustal structure, one may obtain estimates of the Moho heat flow between 11 and 15 mW m^{-2} throughout the Canadian Shield [*Pinet et al.*, 1991; *Jaupart et al.*, 1998]. In order to further constrain crustal compositional models, *Guillou et al.* [1994] used seismic refraction, gravity, and heat flow data. They concluded that the mantle heat flow is between 7 and 15 mW m^{-2}. Independent heat flow studies in large areas of low heat flow over depleted crust in the Superior Province lead to estimates between 10 and 15 mW m^{-2} [*Mareschal and Jaupart*, 2004]. Studies on mantle xenoliths from Kirkland Lake, in the Superior Province, suggest values of 15–18 mW m^{-2} [*Rudnick and Nyblade*, 1999; *Michaut and Jaupart*, 2004]. These various ranges reflect uncertainties in the data and interpretation methods and do not correspond to the magnitude of lateral variations. Our preferred value for Moho heat flow is 15 mW m^{-2} because it is consistent with both heat flow and xenolith data.

[13] For given values of heat flow at the surface and at the Moho, one may deduce the total crustal heat production but not the vertical distribution of the radioelements. For the purposes of calculating temperatures at the Moho, variability of heat production on the scale of individual geological units (~10–20 km) is irrelevant and one must consider an average heat production model. In the southern Superior Province, *Perry et al.* [2006] have studied in detail the distributions of heat flow and heat production. They demonstrated that the crusts of the volcano-plutonic belts (Wawa, Wabigoon, and Uchi) are poorly stratified, such that the vertical average of heat production is very close to the surface average. This is supported by geophysical, petrological and geological studies, which indicate that enriched granitoids account for a significant fraction of the rock types at all crustal levels. In contrast, the intervening metasedimentary belts (English River and Quetico) are characterized by significantly higher values of heat production at the surface and only slightly higher values of heat flow. In these narrow belts, radioelements are enriched in the upper crust. Crustal structure is more complicated, but well documented, in the Abitibi subprovince. The standard model in this subprovince calls for 3 crustal layers of variable thickness: the greenstone volcanics at the surface, an intermediate layer of tonalitic composition, and a granulitic lower crust [*Pinet et al.*, 1991; *Guillou et al.*, 1994; *Mareschal et al.*, 2000]. The heat production in each of these layers is well constrained as they have been extensively sampled, in particular near the Kapuskasing structure where a nearly complete crustal section is exposed [*Ashwal et al.*, 1987; *Shaw et al.*, 1994]. As a general rule, the shallower the heat sources, the lower the Moho temperature. The main contribution to the surface heat flow comes from the intermediate layer of tonalitic gneisses while the upper and lower crust are depleted in radioelements [*Pinet et al.*, 1991]. The difference in Moho temperature between a homogeneous crust and a three layer crust (with the highest heat production in the intermediate crust) is ~25 K, which may be considered negligible.

[14] We carry out calculations for a uniform vertical distribution of heat production in all areas and evaluate a posteriori the validity of the results. This serves to assess the reliability of the thermal models. As discussed above, it is appropriate to assume that the radioelements are uniformly distributed in many belts of the Superior Province. For a constant crustal thermal conductivity k_c = 2.5 W $m^{-1}K^{-1}$, the Moho temperature T_m may be written as

$$T_m = \left(\frac{Q_s + Q_m}{2k_c}\right) h_c \tag{1}$$

where Q_s and Q_m are the surface and Moho heat flow, respectively, and h_c is the crustal thickness. The temperature at the Moho calculated in this way is shown in Figure 5 for an assumed Moho heat flow of 15 mW m^{-2}. This model will be referred to as model A.

3.2. Temperature Dependence of Thermal Conductivity

[15] Within the range of crustal temperatures, thermal conductivity varies significantly, which must be taken into account for accurate temperature estimates. Measurements by *Durham et al.* [1987] are especially applicable to our study as many of their rock samples came from the Superior Province. They determined thermal diffusivity of a wide range of different types of igneous rocks at temperatures and pressures up to 700 K and 200 MPa, respectively. At these temperature and pressure conditions, lattice conduction (phonon transport) is the dominant mechanism of heat transport. *Durham et al.* [1987] obtained the following equation as a best fit for all their measurements of thermal diffusivity α (in mm^2 s^{-1}):

$$\alpha = 0.47 + 78T^{-1} - 1.31\lambda_Q + 1540\lambda_Q T^{-1} \tag{2}$$

where T is absolute temperature and λ_Q is the volume fraction of quartz in the whole rock. For the pressure range of crustal studies, pressure effects can be ignored without introducing significant error. The average conductivity for all the surface samples in the Superior Province is 3 W m^{-1} K^{-1} at room temperature. We have taken ρ = 2700 kg m^{-3} and C_p = 1.2 kJ kg^{-1} K^{-1}, and determined λ_Q as a function of the surface thermal conductivity k_o. Granulite facies rocks which are representative of lower crustal lithology have thermal conductivities between 3.0 and 3.5 W m^{-1} K^{-1} at room temperature [*Jõeleht et al.*, 1998], and therefore the same conductivity equation may be used

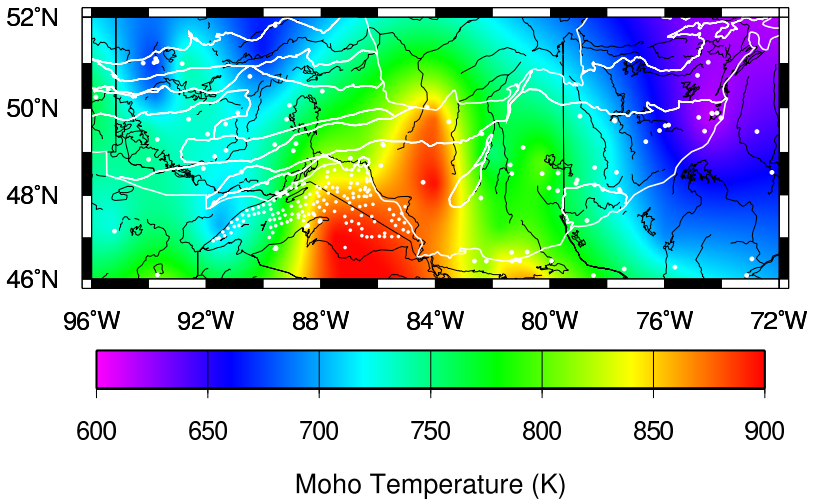


Figure 5. Absolute temperature at the Moho calculated for model A (constant thermal conductivity k = 2.5 W m^{-1} K^{-1}, uniform crustal heat production, and an imposed Moho heat flow Q_m = 15 mW m^{-2}). Results are smoothed to 0.05° × 0.05°. The large white circles show the land heat flow measurement sites. The small white circles are lake heat flow sites from *Hart et al.* [1994]. The white lines mark the subprovince geological boundaries of the Superior Province.

throughout the crust. Our expression for the thermal conductivity is

$$k(T) = 2.264 - \frac{618.2}{T} + k_o\left(\frac{355.6}{T} - 0.3025\right) \quad (3)$$

where k_o = 3.0 W m^{-1} K^{-1}. Equation (3) gives an average conductivity value of 2.0 W m^{-1} K^{-1} in the lower crust.

[16] Radiative heat transport becomes important for temperatures higher than 700–800 K and results in increasing the effective conductivity [*Roy et al.*, 1981; *Clauser and Huenges*, 1995]. Laboratory experiments have been carried out on mantle minerals at temperatures above 1000 K [*Schatz and Simmons*, 1972; *Schärmeli*, 1979; *Roy et al.*, 1981]. The radiative component of thermal conductivity obeys the following law:

$$k = cT^3 \quad (4)$$

where the coefficient c = 0.37 × 10^{-9} W m K^{-4} [*Schatz and Simmons*, 1972; *Schärmeli*, 1979]. Conductivity is thus taken as the sum of lattice and radiative components.

[17] Our working model for the Superior Province is the homogeneous crustal heat production, with a constant heat production equal to $(Q_s - Q_m)/h_c$. The Moho temperature is obtained by integrating the heat conduction equation:

$$k(T)\frac{dT}{dz} = Q_s + (Q_m - Q_s)\frac{z}{h_c} \quad (5)$$

where $k(T)$ is given by equations (3) and (4). Accounting for temperature-dependent thermal conductivity increases the Moho temperature by as much as ~150 K. The results are shown in Figure 6 and will be referred to as model B. The Moho temperatures calculated for different values of Moho heat flow ($0 \le Q_m \le 25$ mW m^{-2}) range between ~600 and 1200 K, with the highest Moho heat flow producing the highest Moho temperatures. Model B is our preferred model for Moho temperature.

4. Correlation Between Moho Temperature and P_n Velocity

4.1. An Empirical Temperature Derivative for P_n Velocity

[18] This study involves many independent input variables. In this case, brute force error analysis based on the addition of individual uncertainties leads to very large error estimates. To circumvent this problem, we proceed in two steps. Temperature calculations rely on values for the surface heat flow, mantle heat flow, thermal conductivity and on the vertical distribution of heat production. For 2° × 2° cells that contain more than 2 heat flow sites, uncertainties on surface heat flow values are small, typically <5%, and their impact on the Moho temperature may be neglected. We assume that thermal conductivity does not introduce significant errors because of the excellent laboratory measurements of *Durham et al.* [1987]. As discussed above, the large geophysical and geochemical data set available in the study area allows strong constraints on the vertical distribution of radioelements and the associated temperature uncertainties are small, ~25 K. We are thus left with the Moho heat flow as the main potential source of error. From Table 1, varying the Moho heat flow by 5 mW m^{-2} leads to a change in Moho temperature of ~50 K. The key point is that, although its absolute value is not known precisely, the Moho heat flow cannot vary by more than ~2 mW m^{-2} across the study area. Two recent studies have elaborated on this in detail and need not be repeated here [*Mareschal and Jaupart*, 2004; *Perry et al.*, 2006]. We thus take a single value of Q_m throughout the study area and use it as the control variable for uncertainties on temperature. In a second step developed later, we address the difficulty of working with a small range of P_n velocities.

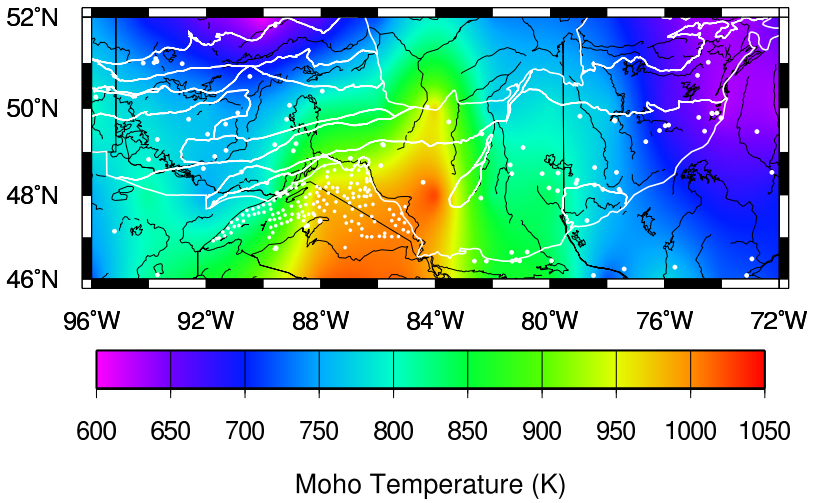


Figure 6. Absolute temperature at the Moho calculated for model B (temperature-dependent thermal conductivity, uniform crustal heat production, and an imposed Moho heat flow Q_m = 15 mW m^{-2}). Results are smoothed to 0.05° × 0.05°. The large white circles show the land heat flow measurement sites. The small white circles are lake heat flow sites from *Hart et al.* [1994]. The white lines mark the subprovince geological boundaries of the Superior Province.

[19] P_n velocities are weakly correlated to surface heat flow (see Figure 7) but very well correlated to predicted Moho temperatures for all values of Q_m (see Table 1 and Figure 8). These data can be used to calculate the derivative $A = \partial V(P_n)/\partial T$ through a least squares procedure. The intercepts γ, the slopes A, and the correlation coefficients for the best fit linear regression through the (P_n, T_m) array are listed in Table 2. The scatter around the best fit linear regression is about ±30 K, which may be accounted by local variations in the vertical distribution of radioelements.

Table 1. Average P_n Velocity, Crustal Thickness, Surface Heat Flow, and Moho Temperature Calculated From Surface Heat Flow Measurements[a]

					T,[c] K				
Longitude, °W	Latitude, °N	H_c, km	P_n Velocity, km s−1	Q_s,[b] mW m^{-2}	Q_m = 0 mW m^{-2}	Q_m = 15 mW m^{-2}	Q_m = 25 mW m^{-2}	N_Q	N_{Pn}
94	50	38.0	8.29 ± 0.03	45.8	635	778	878	5	3
92	50	40.5	8.29 ± 0.03	40.6	612	763	869	4	3
90	50	41.5	8.21 ± 0.02	38.6	602	755	863	4	6
88	50	45.2	8.04 ± 0.04	39.7	648	820	940	2	3
84	50	43.8	8.04 ± 0.05	54.0	792	968	1090	2	2
82	50	44.8	8.06 ± 0.05	33.0	607	773	891	1	2
80	50	42.7	8.16 ± 0.03	40.2	630	790	903	2	3
78	50	40.7	8.20 ± 0.10	40.8	616	768	874	1	1
92	48	43.0	8.23 ± 0.10	36.3	592	750	862	10	1
90	48	46.3	8.15 ± 0.05	35.7	614	788	910	34	2
88	48	52.9	8.05 ± 0.10	43.3	774	986	1134	55	1
86	48	52.1	8.03 ± 0.10	44.5	780	989	1136	33	1
84	48	50.7	8.05 ± 0.04	48.8	821	1027	1170	2	3
82	48	41.6	8.12 ± 0.03	45.2	669	829	940	3	5
80	48	42.9	8.16 ± 0.01	44.1	672	836	952	6	13
78	48	41.2	8.20 ± 0.03	39.4	607	760	868	7	4
76	48	38.0	8.21 ± 0.10	39.5	578	716	814	1	1
94	46	42.6	8.23 ± 0.10	42.6	653	815	928	2	1
90	46	47.3	8.12 ± 0.10	45.1	732	919	1049	2	1
88	46	49.9	8.06 ± 0.07	48.6	808	1010	1150	3	2
82	46	39.4	8.20 ± 0.02	51.4	705	858	965	7	7
80	46	44.9	8.20 ± 0.03	43.0	683	856	977	3	4
78	46	42.4	8.20 ± 0.02	34.0	564	718	828	4	5
76	46	38.5	8.20 ± 0.10	45.1	634	779	880	2	1
74	46	38.6	8.18 ± 0.05	39.2	581	722	822	2	2

[a] H_c is the crustal thickness, Q_s is the surface heat flow, T is the Moho temperature, N_Q and N_{Pn} are the number of heat flow measurements and the number of tabulated shot points from the refraction data in each 2° × 2° cell. See text for explanations of temperature calculation.

[b] Error associated with the determination of surface heat flow is <2 mW m^{-2}.

[c] Error associated with Moho temperature calculations for a given value of the Moho heat flow is ±25 K, due to uncertainties in the vertical distribution of radiogenic heat production. Errors quoted for the average P_n velocity were determined from the supposed error (±0.1 km s^{-1}) on each velocity determination and the dispersion of values within each cell.

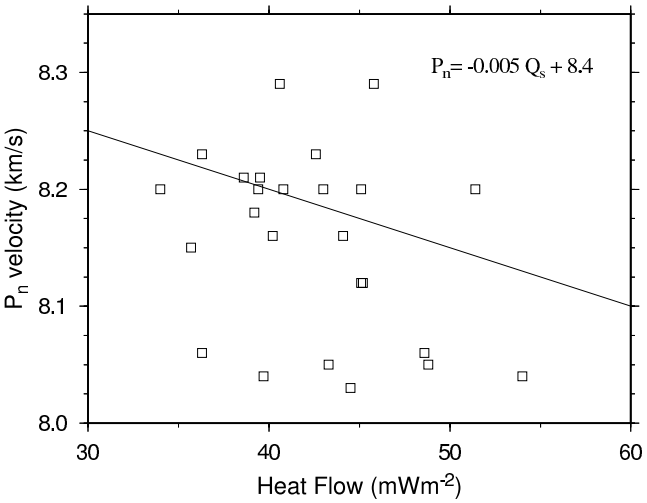


Figure 7. Relationship between P_n velocity and surface heat flow. The correlation is poor.

The fact that observed P_n velocity is better correlated (in absolute value) with calculated Moho temperature than with surface heat flow gives further credence to the thermal model.

[20] The empirical temperature derivative of velocity is insensitive to the value of the Moho heat flow. Excluding solutions for zero Q_m, which are not realistic, this derivative is $-6.0 \times 10^{-4} \pm 10\%$ km s^{-1} K^{-1} for a large range of Moho heat flows ($7 \leq Q_m \leq 25$ mW m^{-2}). This result is within the range of values for ultramafic rocks determined in the laboratory (Table 3). The agreement between the empirical velocity derivative deduced from geophysical data and laboratory measurements shows that variations of P_n velocities in the Superior Province are indeed due to temperature. Below, we proceed further and make a direct comparison with P_n velocities calculated for specific upper mantle compositions. This comparison allows constraints on both the composition of the upper mantle beneath the Superior Province and the Moho heat flow.

4.2. Anomalous Data Points

[21] Four data points (corresponding to four cells in Figures 3 and 6) stand out as anomalies in a plot of P_n velocity as a function of Moho temperature (Figure 8). The triangles correspond to two cells in the northwestern part of the study area including the English River metasedimentary subprovince (centered at 50°N, 92°W and 50°N, 94°W). A third anomalous cell (identified by a cross symbol and corresponding to 50°N, 88°W) straddles the northeast extremity of the Nipigon Embayment, where mafic intrusives associated with the Keweenawan Mid-Continent rift are present in the crust. The fourth outlier cell (identified by a star symbol and centered at 50°N, 82°W) corresponds to the Kapuskasing heat flow site. Here, we show why these four data points show up as anomalies with respect to the others. In all cases, the problem comes from inadequate heat flow sampling of the heterogeneous crust.

[22] The two anomalous cells in the northwestern corner of the study area encompass the Uchi and Wabigoon volcano-plutonic belts and the English River metasedimentary belt, which have different crustal structures, as discussed above. It is difficult to propose an average crustal model valid for such a geological assemblage. One key factor is that the metasedimentary belts have an enriched upper crust which is not accounted for by the homogeneous crustal model. With the same values of heat flow at the surface and at the Moho, an enriched upper crust could diminish the Moho temperature by as much as 100 K. Accounting for this would bring the Moho temperature for these two areas close to the trend defined by the other points.

[23] The third anomalous cell is located at the edge of the Nipigon Embayment, where late stage mafic intrusions occurred during the Keweenawan rifting event ~1100 Ma [*van Schmus et al.*, 1982]. The two heat flow values for this cell are obtained through a mafic intrusive sequence and are rather low. The cell includes parts of the English River and Quetico belts which are both associated with high heat flows (48 mW m^{-2} [*Perry et al.*, 2006]). The low heat low values can be explained by the abundance of depleted mafic rocks in the crust [*Perry et al.*, 2005] and is not representative of areas that are unaffected by the Keweenawan event. It is thus likely that the average heat flow for the cell is higher than the two determinations available. With a heat flow of 48 mW m^{-2}, as elsewhere in the English River and Quetico belts, the Moho temperature is increased by ~100 K, which would remove the anomaly.

[24] The fourth anomalous cell lies in the Kapuskasing uplift region, where depleted lower crustal assemblages have been brought to the surface along a thrust fault [*Percival and Card*, 1983; *Percival and West*, 1994]. The single heat flow determination available for this cell was

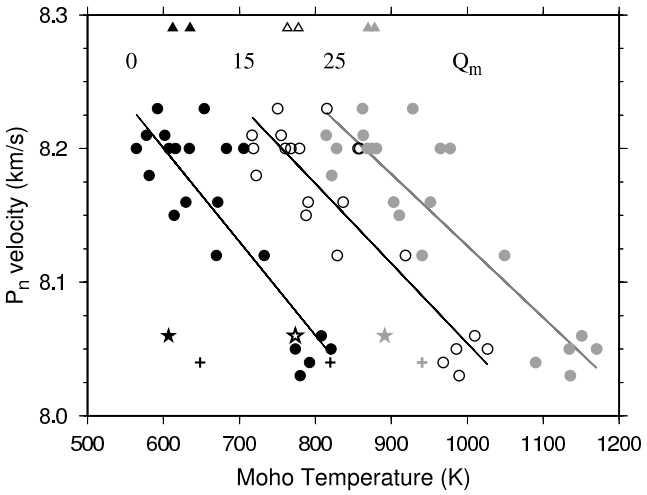


Figure 8. Relationship between P_n velocity and temperature at the Moho. Moho temperature is calculated for three imposed Moho heat flows of 0, 15, and 25 mW m^{-2}. Triangles, crosses, and stars represent the outliers to the trend. The triangles correspond to heat flow sites located in the Uchi subprovince (50°N, 92°W) and (50°N, 94°W), where deep crustal structure is poorly known. The crosses correspond to a heat flow site which neighbors the Nipigon Embayment (50°N, 88°W) where mafic intrusives are present in the lithology. The stars correspond to the Kapuskasing heat flow site (50°N, 82°W).

Table 2. Correlation Between Moho Temperature, Surface Heat Flow, and P_n Velocity[a]

Regression Variables	N	Q_m, mW m^{-2}	$-dV(P_n)/dT$, $\times 10^{-4}$ km s^{-1} K^{-1}	γ	r	α
$T_m - P_n$	25	0	7.0	8.6	−0.685	0.2E-3
$T_m - P_n$	25	7	6.5	8.6	−0.707	0.1E-3
$T_m - P_n$	25	12	6.2	8.6	−0.719	0.1E-3
$T_m - P_n$	25	15	6.0	8.7	−0.726	0.00
$T_m - P_n$	25	25	5.4	8.7	−0.743	0.00
$Q_s - P_n$	64		5.0[b]	8.4	−0.311	0.13

[a] N is the number of data, Q_m is the imposed Moho heat flow, $dV(P_n)/dT$ is the P wave-temperature conversion at Moho depth, γ is the y intercept of the linear regression, r is the correlation coefficient, and α is the level of significance or the probability of getting a correlation as large as the observed value by random chance when the true correlation is zero. The correlation between Moho temperature T_m and P_n velocity is much greater than that between surface heat flow Q_s and P_n velocity. See text for explanations of temperature calculation. The results are plotted in Figures 7 and 8. Read 0.2E-3 as 0.2 × 10−3.

[b] For $-dV(P_n)/dQ_s$ in $\times 10^{-3}$ km s^{-1} mW^{-1} m^2.

measured through such depleted crust and is very low (33 mW m^{-2}). As in the previous case, accounting for the other rock types and types of crust present in the cell would increase the heat flow and the Moho temperature. In this case, because of the very low heat flow value, the correction to the Moho temperature is likely to be large.

[25] This discussion shows that anomalies in the general trend of P_n as a function of Moho temperature can all be accounted for. It further illustrates the necessity of accurate crustal models.

4.3. Error Analysis

[26] P_n velocities are determined with an accuracy of about ±0.1 km s^{-1} according to *Musacchio et al.* [2004]. Errors on crustal thickness are estimated to be between 5 and 10%, but these have no significant impact on P_n velocities, as shown in our previous discussion of pressure effects on seismic wave speeds. The large instrumental error on P_n velocities may seem overwhelming because it is almost as large as the total variation over the study area. For the purposes of this study, however, one can get around this problem.

[27] We first note that, if ±0.1 km s^{-1} were an accurate estimate of the true error on P_n velocity determinations, it would lead to random variations across the study area. In contrast, the data exhibit remarkable large-scale spatial coherence, including cells sampled by independent seismic surveys. One gets better statistics on P_n velocities by accounting for the number of individual determinations per cell, which may be as large as 13. Table 1 lists errors on the cell-averaged P_n velocity. Uncertainties were calculated from both the dispersion of individual determinations within a cell and the measurement error, and are small in cells with a large number of data points. One could reduce uncertainties by carrying out a more sophisticated spatial correlation analysis. Another method to reduce the uncertainties would be to impose the experimental value of the temperature derivative of wave speed, which is well-known for given mineral assemblages. One could thus use the empirical (P_n, T) array to calculate a best fit anchor point with a small uncertainty.

[28] For this study, such refinements are not necessary. On one hand, we are dealing with a rather restricted range of rock compositions for which the temperature derivative of seismic velocity varies little, as will be shown below. On the other hand, the slope of the empirical (P_n, T) arrays (the temperature derivative of wave speed) is not sensitive to the single control variable (the Moho heat flow) and takes values that are close to laboratory results. Thus, in effect, we seek to compare two parallel arrays, one deduced from laboratory data and the other derived from geophysical measurements, and one needs only to focus on their respective anchor points and the associated control variables: the compositional model and the Moho heat flow.

5. Comparison With a Mineralogical Model for the Upper Mantle

5.1. Calculation of *P* Wave Velocity

[29] Calculating the P wave velocity of a mantle mineral assemblage for in situ conditions requires several inputs: the mantle composition, the thermoelastic properties of individual mantle minerals and a correction for anharmonic and anelastic effects [*Shapiro and Ritzwoller*, 2004]. Both P and S wave velocity-temperature curves have two distinct, almost linear parts: the anharmonic domain (temperatures

Table 3. Temperature Derivatives of P Wave Velocity in Upper Mantle Rocks[a]

Sample	$-dV_P/dT$, $\times 10^{-4}$ km s^{-1} K^{-1}	T, °C	P, MPa	Reference
Peridotite	4.4	400–700	410	*Fielitz* [1976]
Peridotite, Ivrea Zone, Italy	4.9[b]	20–500	600	*Kern and Richter* [1981]
Lherzolite xenoliths, Sierra Nevada	6.2–6.9[c]	25–260	300–900	*Peselnik et al.* [1977]
Harzburgite, Antalya ophiolite, Turkey	5.6–6.7[d]	25–275	200–800	*Peselnik and Nicolas* [1978]
Lherzolite xenolith, Hawaii	6.7–7.1[d]	25–275	200–800	*Peselnik and Nicolas* [1978]

[a] T and P stand for the temperatures and pressures achieved.

[b] Mean value for measurements in 3 orthogonal directions.

[c] Range for two different samples with different olivine fabrics.

[d] Range for measurements in three orthogonal orientations.

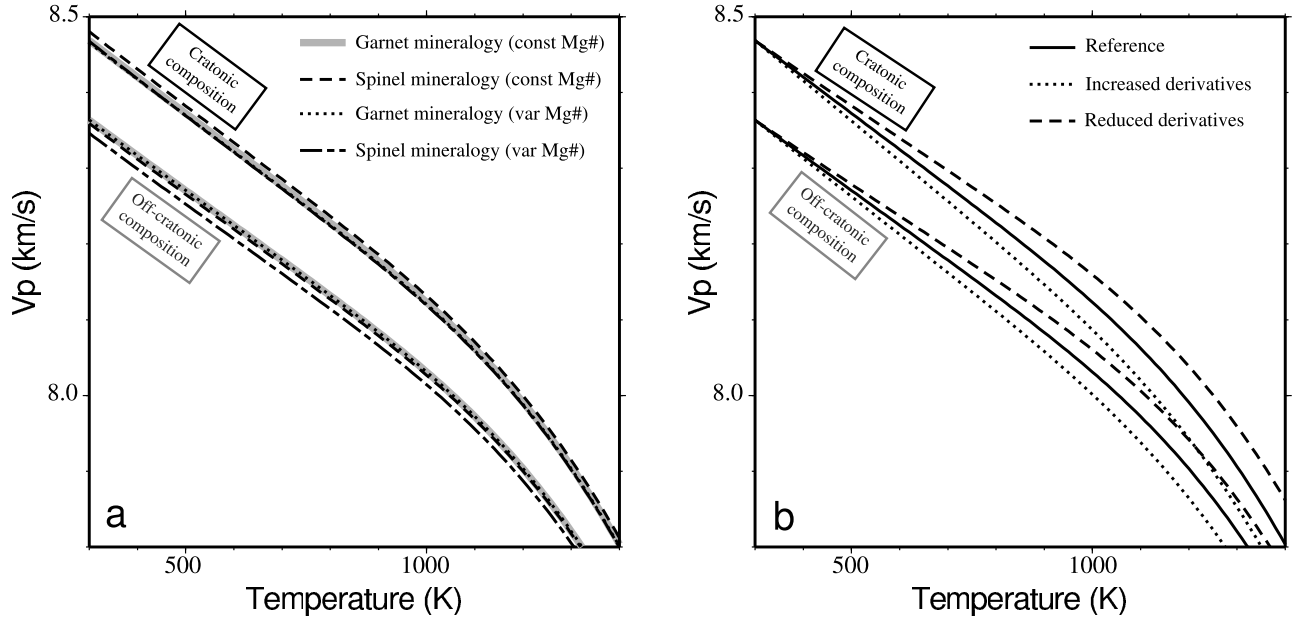


Figure 9. *P* wave velocity and temperature calculated for on-craton and off-craton composition (Table 4). (a) Results for two different mineralogical facies (garnet-lherzolite and spinel-lherzolite) and two models of the Fe/Mg distribution within minerals. Details of mineralogical compositions and Mg # variations are given by *McDonough and Rudnick* [1998]. (b) Effect of uncertainties in $\partial\mu/\partial T$ and $\partial K/\partial T$ for olivine. "Increased" and "reduced" derivatives correspond to the upper and lower bounds reported by *Goes et al.* [2000].

<1000°C) and the anelastic domain for temperatures >1000°C, with a narrow transition zone between the two [*Shapiro and Ritzwoller*, 2004]. Anelastic effects are only important at temperatures exceeding 1000°C [e.g., *Karato*, 1993] and hence are neglected because Moho temperatures are less than this threshold value. We have not allowed for the presence of free melt and/or water phases in the mantle, which reduce mantle seismic velocities through enhanced anelasticity [*Karato and Jung*, 1998]. We note that the calculated Moho temperatures are too low for mantle melting to occur. *Griffin et al.* [2004] found evidence for many episodes of fluid introduction (metasomatism) in the North American continental lithosphere. Such rehydration binds the fluid components within mineral phases which should have less effect on seismic velocity than free fluids.

[30] To investigate errors in *P* wave velocity calculations due to uncertainties in elastic parameters, we used a recent compilation of laboratory data of seismic velocity and velocity derivatives [*Goes et al.*, 2000]. These errors have been explored for a particular set of upper mantle models [*McDonough and Rudnick*, 1998] and are illustrated in Figure 9. First, we found that the temperature-seismic velocity conversion depends weakly on the mineralogical facies (spinel versus garnet mineralogy) and on the Fe/Mg distribution among different minerals (Figure 9). Second, we found that uncertainties in the derivatives of the shear modulus $\partial\mu/\partial T$ and the bulk modulus $\partial K/\partial T$ for olivine have the greatest effect on the calculated velocities. We shall vary these derivatives within the range of experimental data reported by *Goes et al.* [2000].

[31] Variations of seismic velocity due to changes of the bulk mantle mineralogical composition are significant. Matching observed and calculated P_n velocities therefore yields constraints on the bulk upper mantle composition. Differences in chemical composition of the upper mantle amongst geological provinces or between entire continents have been established by *McDonough and Rudnick* [1998] and *Griffin et al.* [2003]. Seismic-geodynamic inversions have placed constraints on the degree of iron depletion in the upper mantle [e.g., *Forte and Perry*, 2000; *Perry et al.*, 2003; *Godey et al.*, 2004; *van Gerven et al.*, 2004] and yielded values of Mg # in good agreement with xenolith studies at depths of 150–200 km.

[32] The composition of subcontinental lithospheric mantle varies significantly with both depth and location [*Griffin et al.*, 2003, 2004], but there seems to be a systematic difference between Archean samples and younger ones. Table 4 lists two sets of compositional models that are widely used. *McDonough and Rudnick* [1998] have compiled data from kimberlites and alkali basalt

Table 4. Mineralogical Composition of Continental Lithospheric Mantle[a]

	Ol, %	Opx, %	Cpx, %	Gt, %	Mg #	Reference
On-craton	83	15	0	2	91.4	*McDonough and Rudnick* [1998]
Off-craton	68	18	11	3	89.8	*McDonough and Rudnick* [1998]
Archon	69	25	2	4	92.7	*Griffin et al.* [2003]
Proton	70	17	6	7	90.6	*Griffin et al.* [2003]

[a]Ol, olivine; Opx, orthopyroxene; Cpx, clinopyroxene; Gt, garnet.

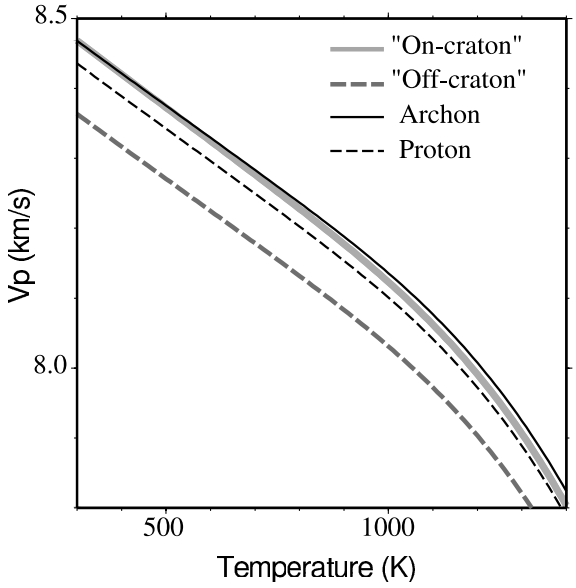


Figure 10. Relationship between *P* wave velocity and temperature following the method of *Shapiro and Ritzwoller* [2004]. Mineralogical compositions are based on the work by *McDonough and Rudnick* [1998] and *Griffin et al.* [2003] (see Table 4). The difference in *P* wave velocity between on-craton and off-craton models is 2%.

intrusives to derive an average model for Archean lithospheric mantle which they called "on-craton." They further obtained an "off-craton" model for Proterozoic and younger continental regions from analyses of massif peridotites, which may be found at Earth's surface in many Phanerozoic fold belts. *Griffin et al.* [2003] noted that xenolith data are heavily biased toward southern African kimberlites and added a large data set of xenocrysts carried by alkali basalts. They derived average compositions of Archean and Proterozoic samples, corresponding to "Archons" and "Protons" respectively. The two different sets of models share many characteristics such as clinopyroxene depletion in the Archean and modal contents for off-craton and Proton samples. As shown by Figure 10, the relationship between V_p and temperature for the off-craton model falls far from those of the other three models. We do not expect that this model is appropriate for our study area but will use it to demonstrate that the data can indeed rule it out. Surprisingly, the on-craton and Archon models yield (V_p, T) curves that are almost identical despite their large modal differences and their different values of Mg #. The Proton model is shifted from the two Archean models in the direction of the off-craton model (Figure 10). Note that the temperature derivatives are slightly different for the two types of mantle composition. Compositional differences have the strongest effect at low temperature and affect *P* wave velocity more than *S* wave velocity.

5.2. Results

[33] We compare our $V_P - T$ relationship with those of the calculated mineralogical models using the methods of *Goes et al.* [2000] and *Shapiro and Ritzwoller* [2004] (Figure 11). There is good agreement between observations and predictions for Archean and Proterozoic models of the lithospheric upper mantle. Within the error limits of

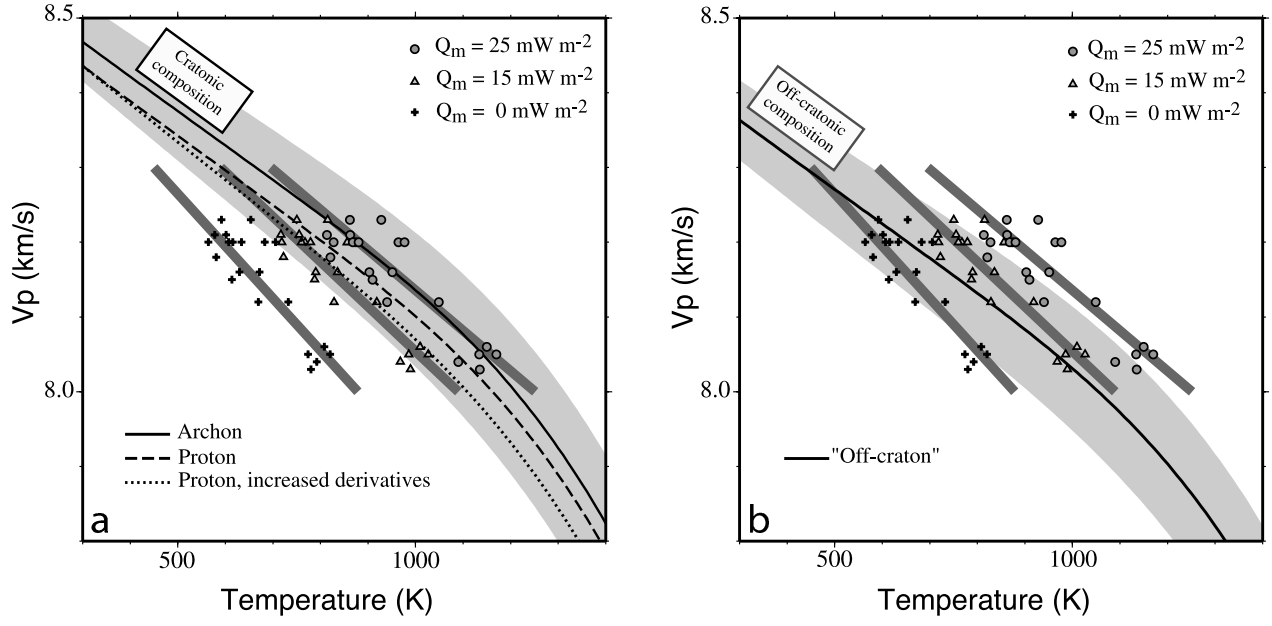


Figure 11. Relationship between *P* wave velocity and temperature at the Moho for (a) various models of craton composition and (b) the off-craton composition. The sum of the errors associated with the upper mantle composition and the elastic derivatives is shown by the gray shaded zones and amounts to about ±1%. Crosses, triangles, and circles are (P_n, T) pairs from seismic refraction and heat flow data for heat flows of 0, 15, and 25 mW m^{-2}, respectively. The P_n velocity-temperature values for a Moho heat flow of 15 mW m^{-2} (the preferred solution) are clearly consistent with calculated velocities for an Archean upper mantle mineralogy.

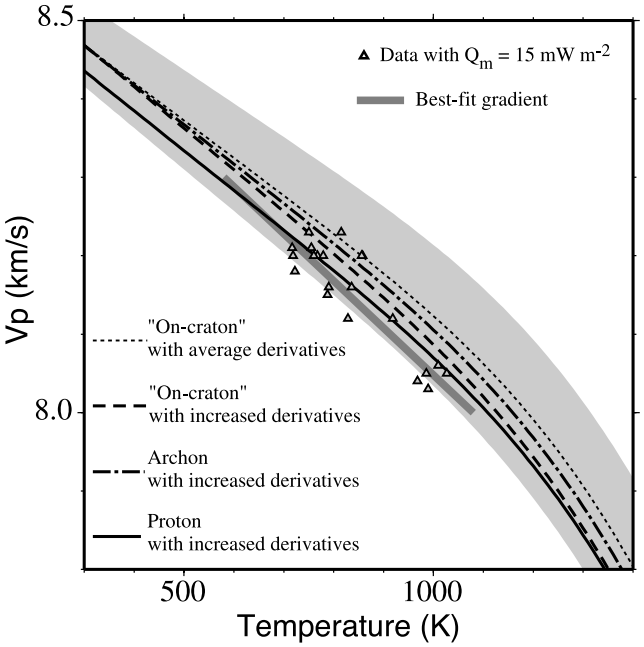


Figure 12. Relationship between P wave velocity and temperature at the Moho. Triangles are (P_n, T) pairs from seismic refraction and Moho temperature calculated for a Moho heat flow of 15 mW m^{-2}. The dark gray shaded line is the best fit linear relationship for this large-scale geophysical data set. The sum of the errors associated with upper mantle composition and elastic derivatives is represented by the shaded gray zone. The dotted line is the P wave velocity-temperature correlation for the compositional model of *McDonough and Rudnick* [1998], and the dashed line is the correlation for their compositional model with increased elastic derivatives. The solid and dash-dotted lines correspond to the compositional model of *Griffin et al.* [2003] for Archons and Protons, respectively, with increased elastic derivatives.

these mineralogical models, mantle heat flow must be at least 12 mW m^{-2}, which is consistent with the independent constraints discussed above. Neither the surface heat flow and heat production data, nor the xenolith data from the Superior Province can justify Moho heat values greater than 18 mW m^{-2} [*Perry et al.*, 2006]. The velocity-temperature relationship for $12 \leq Q_m \leq 18$ mW m^{-2} is consistent with the mineralogical models. The agreement between the observed and predicted curves is improved by using the largest values of $\partial\mu/\partial T$ and $\partial K/\partial T$ that are compatible with laboratory data. The off-craton model does not allow a satisfactory fit to the data, as expected, mostly because the implied temperature derivative is too high. This shows the sensitivity of the data to the upper mantle composition.

[34] We may proceed further by tightening the range of Moho heat flow values, bearing in mind that none of the xenolith or xenocryst data provide information on depths shallower than about 80 km. Figure 12 and Table 4 show our preferred thermal model, where Q_m = 15 mW m^{-2}. Given the uncertainties in both P_n velocities and Moho temperature, the data are in good agreement with predictions for Archean and Proterozoic craton compositions. The data are closer to the Proton curve (Figure 12), which seems to be in contradiction with the Archean age of the Superior Province. We must remember, however, that this craton was subjected to two perturbations during the Proterozoic, which have led to the emplacement of numerous dykes near the Kapuskasing uplift and the Keweenawan rift. The Kyle Lake and Attawapiskat kimberlites, to the north of the study area, have yielded samples of the shallow lithospheric mantle (~95 km depth) that are fertile lherzolites [*Griffin et al.*, 2004]. Such compositions do not match the "Archon" model. Garnet minerals from the Sextant Rapids melilitite, within the Kapuskasing Structural Zone, also correspond to fertile lherzolite compositions [*Griffin et al.*, 2004]. These data indicate that the Archean lithospheric mantle beneath the study area has been modified by melt-related metasomatic fluids. Such modification acts to shift the upper mantle composition toward Proton values, which is consistent with our preferred values of the Moho heat flow. The Proton composition consists of a mantle that is less depleted in olivine and has a smaller Mg # (90.6) than the Archon composition (Table 4). *Perry et al.* [2003] used the tomographic model of *Grand et al.* [1997] and predicted an average Mg # of ~91 in the region of the Superior Province at 150 km depth, based on cratonic-scale seismic-geodynamic inversions of geophysical observables. However, Mg # was shown to be depth-dependent in the North American lithospheric mantle [*Griffin et al.*, 2004]. Such detailed considerations must be regarded as tentative because of the uncertainties involved, but they illustrate how the combination of heat flow and P_n velocity data can constrain the shallow upper mantle composition which is rarely sampled.

6. Conclusions

[35] P_n velocities from seismic refraction data are well correlated with temperature at the Moho derived from heat flow data. The combination of the two data sets (Moho temperature, P_n velocities) allows a test of the mineralogical composition used in models for tomographic inversions. We calculated temperature and P_n velocity for various mineralogical models of the upper mantle and compared the results to the ($P_n - T_m$) couples from seismic refraction and heat flow. This comparison demonstrates that the theoretical velocity-temperature conversion used for interpretation of seismic tomographic models is in good agreement with observations. Our preferred solution, which combines constraints on the Moho heat flow as well as on the composition of the lithospheric mantle, has a Moho heat flow of 15 mW m^{-2} and a slightly depleted mantle composition with a Mg # equal to 91.

[36] **Acknowledgments.** We thank D. Eaton for fruitful discussions during the initial stages of this work. J. Percival is thanked for kindly providing the Superior Province polygons. Constructive comments by W. Griffin, the Associate Editor, and an anonymous reviewer greatly improved the quality of the manuscript. H. K. C. Perry was the recipient of an NSERC graduate scholarship. This research was supported by INSU (CNRS, France) and by NSERC (Canada).

References

Ashwal, L. D., P. Morgan, S. A. Kelley, and J. Percival (1987), Heat production in an Archean crustal profile and implications for heat flow

and mobilization of heat producing elements, *Earth Planet. Sci. Lett.*, *85*, 439–450.

Black, P. R., and L. W. Braile (1982), P_n velocity and cooling of the continental lithosphere, *J. Geophys. Res.*, *87*, 10,557–10,568.

Christensen, N. I. (1974), Compressional wave velocity in possible mantle rocks to pressures of 30 kilobars, *J. Geophys. Res.*, *79*, 407–412.

Chung, D. J. (1977), P_n velocity and partial melting: Discussion, *Tectonophysics*, *42*, T35–T42.

Clauser, C., and E. Huenges (1995), Thermal conductivity of rocks and minerals, in *Rock Physics and Phase Relations: A Handbook of Physical Constants*, *AGU Ref. Shelf*, vol. 3, edited by T. J. Ahrens, pp. 105–126, AGU, Washington, D. C.

Clowes, R. M., F. Cook, Z. Hajnal, J. Hall, J. Lewry, S. Lucas, and R. Wardle (1999), Canada's Lithoprobe Project: Collaborative, multidisciplinary geoscience research leads to new understanding of continental evolution, *Episodes*, *22*, 3–20.

Debayle, E., and B. L. N. Kennett (2000), Anisotropy in the Australian upper mantle from Love and Rayleigh waveform inversion, *Earth Planet. Sci. Lett*, *184*, 339–351.

Durham, W. B., V. V. Mirkovich, and H. C. Heard (1987), Thermal diffusivity of igneous rocks at elevated pressure and temperature, *J. Geophys. Res.*, *92*, 11,615–11,634.

Fielitz, K. (1976), Compressional and shear wave velocities as a function of temperature in rocks at high pressure, in *Explosion Seismology in Western Europe*, edited by P. Giese, C. Prodehl, and A. Stein, pp. 40–44, Springer, New York.

Forte, A. M., and H. K. C. Perry (2000), Geodynamical evidence for a chemically depleted continental tectosphere, *Science*, *290*, 1940–1944.

Godey, S., F. Deschamps, J. Trampert, and R. Snieder (2004), Thermal and compositional anomalies beneath the North American continent, *J. Geophys. Res.*, *109*, B01308, doi:10.1029/2002JB002263.

Goes, S., R. Govers, and P. Vacher (2000), Shallow mantle temperatures under Europe from *P* and *S* wave tomography, *J. Geophys. Res.*, *105*, 11,153–11,169.

Grand, S. P., R. D. van der Hilst, and S. Widiyantoro (1997), Global seismic tomography: A snapshot of convection in the Earth, *GSA Today*, *7*, 1–7.

Griffin, W. L., S. Y. O'Reilly, N. Abe, S. Aulbach, R. M. Davies, N. J. Pearson, B. J. Doyle, and K. Kivi (2003), The origin and evolution of Archean lithospheric mantle, *Precambrian Res.*, *127*, 19–41, doi:10.1016/S0301-9268 (03)00180-3.

Griffin, W. L., S. Y. O'Reilly, B. J. Doyle, N. J. Pearson, H. Coopersmith, K. Kivi, V. Malkovets, and N. Pokhilenko (2004), Lithosphere mapping beneath the North American plate, *Lithos*, *77*, 873–922, doi:10.1016/j.lithos.2004.03.034.

Guillou, L., J. C. Mareschal, C. Jaupart, C. Gariépy, G. Bienfait, and R. Lapointe (1994), Heat flow and gravity structure of the Abitibi belt, Superior Province, Canada, *Earth Planet. Sci. Lett.*, *122*, 447–460.

Hart, S. R., J. S. Steinhart, and T. J. Smith (1994), Terrestrial heat flow in Lake Superior, *Can. J. Earth Sci.*, *31*, 698–708.

Herrin, E. (1969), Regional variations of P-wave velocity in the upper mantle beneath North America, in *The Earth's Crust and Upper Mantle*, *Geophys. Monogr. Ser.*, vol. 13, edited by P. J. Hart, pp. 242–246, AGU, Washington, D. C.

Herrin, E., and J. Taggert (1962), Regional variations in P_n velocity and their effect on the location of epicenters, *Bull. Seismol. Soc. Am.*, *52*, 1037–1046.

Horai, K., and G. Simmons (1968), Seismic travel time anomaly due to anomalous heat flow and density, *J. Geophys. Res.*, *73*, 7577–7588.

Jaupart, C., J. C. Mareschal, L. Guillou-Frottier, and A. Davaille (1998), Heat flow and thickness of the lithosphere in the Canadian Shield, *J. Geophys. Res.*, *103*, 15,269–15,286.

Jõeleht, A., I. T. Kukkonen, and G. Pšenčik (1998), Thermal properties of granulite facies rocks in the Precambrian basement of Finland and Estonia, *Tectonophysics*, *291*, 195–203.

Karato, S. (1993), Importance of anelasticity in the interpretation of seismic tomography, *Geophys. Res. Lett.*, *20*, 1623–1626.

Karato, S., and H. Jung (1998), Water, partial melting and the origin of the seismic low velocity and high attenuation zone in the upper mantle, *Earth Planet. Sci. Lett.*, *157*, 193–207.

Kay, I., S. Sol, J. M. Kendall, C. J. Thomson, D. J. White, I. Asudeh, B. Roberts, and D. Francis (1999), Shear wave splitting observations in the Archean Craton of Western Superior, *Geophys. Res. Lett.*, *26*, 2669–2672.

Kern, H., and A. Richter (1981), Temperature derivatives of compressional and shear wave velocities in crustal and mantle rocks at 6 kbar confining pressure, *J. Geophys.*, *49*, 47–56.

Lewis, T. J., R. D. Hyndman, and P. Fuelck (2003), Heat flow, heat generation, and crustal temperatures in the northern Canadian Cordillera: Thermal control of tectonics, *J. Geophys. Res.*, *108*(B6), 2316, doi:10.1029/2002JB002090.

Manghnani, M. H., R. Ramananantoandro, and S. P. Clark (1974), Compressional and shear wave velocities in granulite facies rocks and eclogites to 10 kbar, *J. Geophys. Res.*, *79*, 5427–5446.

Mareschal, J. C., and C. Jaupart (2004), Variations of surface heat flow and lithospheric thermal structure beneath the North American craton, *Earth Planet. Sci. Lett.*, *223*, 65–77.

Mareschal, J. C., C. Jaupart, C. Gariépy, L. Z. Cheng, L. Guillou-Frottier, G. Bienfait, and R. Lapointe (2000), Heat flow and deep thermal structure near the edge of the Canadian Shield, *Can. J. Earth Sci.*, *37*, 399–414.

McDonough, W. F., and R. L. Rudnick (1998), Mineralogy and composition of the upper mantle, in *Ultrahigh-Pressure Mineralogy: Physics and Chemistry of the Earth's Deep Interior*, edited by R. J. Hemley, pp. 139–164, Mineral. Soc. of Am., Washington, D. C.

Michaut, C., and C. Jaupart (2004), Nonequilibrium temperatures and cooling rates in thick continental lithosphere, *Geophys. Res. Lett.*, *31*, L24602, doi:10.1029/2004GL021092.

Musacchio, G., D. J. White, I. Asudeh, and C. J. Thomson (2004), Lithospheric structure and composition of the Archean western Superior Province from seismic refraction/wide-angle reflection and gravity modeling, *J. Geophys. Res.*, *109*, B03304, doi:10.1029/2003JB002427.

Pakiser, L. C. (1963), Structure of the crust and upper mantle in the western United States, *J. Geophys. Res.*, *68*, 5747–5756.

Pakiser, L. C., and J. S. Steinhart (1964), Explosion seismology in the western hemisphere, in *Research in Geophysics*, vol. 2, *Solid Earth and Interface Phenomena*, edited by J. Odishaw, pp. 123–142, MIT Press, Cambridge, Mass.

Percival, J. A., and K. D. Card (1983), Archean crust as revealed in the Kapuskasing uplift, Superior Province, *Geology*, *11*, 323–326.

Percival, J. A., and G. F. West (1994), The Kapuskasing uplift: a geological and geophysical synthesis, *Can. J. Earth Sci.*, *31*, 1256–1286.

Perry, H. K. C., D. W. S. Eaton, and A. M. Forte (2002), A revised crustal model for Canada based on Lithoprobe results, *Geophys. J. Int.*, *150*, 285–294.

Perry, H. K. C., A. M. Forte, and D. W. S. Eaton (2003), Upper-mantle thermochemical structure below North America from seismic-geodynamic flow models, *Geophys. J. Int.*, *154*, 279–299.

Perry, H. K. C., C. Jaupart, J.-C. Mareschal, F. Rolandone, and G. Bienfait (2004), Heat flow in the Nipigon arm of the Keweenawan rift, northwestern Ontario, Canada, *Geophys. Res. Lett.*, *31*, L15607, doi:10.1029/2004GL020159.

Perry, H. K. C., C. Jaupart, J.-C. Mareschal, and G. Bienfait (2006), Crustal heat production in the Superior Province, Canadian Shield, and in North America inferred from heat flow data, *J. Geophys. Res.*, *111*, B04401, doi:10.1029/2005JB003893.

Peselnik, L., and A. Nicolas (1978), Seismic anisotropy in an ophioloite peridotite: Application to the oceanic upper mantle, *J. Geophys. Res.*, *83*, 1227–1235.

Peselnik, L., J. P. Lockwood, and R. M. Stewart (1977), Anisotropic elastic velocities of some upper mantle xenoliths underlying the Sierra Nevada batholith, *J. Geophys. Res.*, *82*, 2005–2010.

Pinet, C., C. Jaupart, J. C. Mareschal, C. Gariépy, G. Bienfait, and R. Lapointe (1991), Heat flow and structure of the lithosphere in the eastern Canadian Shield, *J. Geophys. Res.*, *96*, 19,941–19,963.

Roy, R. F., A. E. Beck, and Y. S. Touloukian (1981), Thermophysical properties of rocks, in *Physical Properties of Rocks and Minerals*, vol. 2, edited by Y. S. Touloukian, W. R. Judd, and R. F. Roy, pp. 409–502, McGraw-Hill, New York.

Rudnick, R. L., and A. A. Nyblade (1999), The thickness of Archean lithosphere: Constraints from xenolith thermobarometry and surface heat flow, in *Mantle Petrology: Field Observations and High Pressure Experimentation: A Tribute to Francis R. (Joe) Boyd*, edited by Y. Fei, C. M. Bertka, and B. O. Mysen, *Spec. Publ. Geochem. Soc.*, *6*, 3–11.

Schärmeli, G. (1979), Identification of radioactive thermal conductivity in olivine up to 25 kbar and 1500 K, paper presented at the 6th AIRAPT Conference, Int. Assoc. for Res. and Adv. of High Pressure Sci. and Technol., Boulder, Colo.

Schatz, J. F., and G. Simmons (1972), Thermal conductivity of Earth materials, *J. Geophys. Res.*, *77*, 6966–6983.

Shapiro, N. M., and M. H. Ritzwoller (2004), Thermodynamic constraints on seismic inversions, *Geophys. J. Int.*, *157*, 1175–1188.

Shaw, D. M., A. P. Dickin, H. Li, R. H. McNutt, H. P. Schwarcz, and M. G. Truscott (1994), Crustal geochemistry in the Wawa-Foleyet region, Ontario, *Can. J. Earth Sci.*, *31*, 1104–1121.

Silver, P. G. (1996), Seismic anisotropy beneath the continents: Probing the depths of geology, *Annu. Rev. Earth Planet. Sci.*, *24*, 385–432.

Silver, P. G., and W. W. Chan (1991), Shear wave splitting and subcontinental mantle deformation, *J. Geophys. Res.*, *96*, 16,429–16,454.

Sobolev, S. V., H. Zeyen, G. Stoll, F. Werling, R. Altherr, and K. Fuchs (1996), Upper mantle temperatures from teleseismic tomography of

French Massif Central including effects of composition, mineral reactions, anharmonicity, anelasticity and partial melt, *Earth Planet. Sci. Lett.*, *157*, 193–207.

van Gerven, L., F. Deschamps, and R. D. van der Hilst (2004), Geophysical evidence for chemical variations in the Australian Continental Mantle, *Geophys. Res. Lett.*, *31*, L17607, doi:10.1029/2004GL020307.

van Schmus, W. R., J. C. Green, and H. C. Halls (1982), Geochronology of Keweenawan rocks of the Lake Superior region: A summary, in *Geology and Tectonics of the Lake Superior Basin*, edited by R. J. Wold and W. J. Hinze, *Mem. Geol. Soc. Am.*, *156*, 165–171.

Vinnik, L. P., I. I. Makayeva, A. Milev, and A. Y. Usenko (1992), Global patterns of azimuthal anisotropy and deformations in the continental mantle, *Geophys. J. Int.*, *111*, 433–447.

Warren, D. H., and J. H. Healy (1973), Structure of the crust in the conterminous United States, *Tectonophysics*, *20*, 203–213.

C. Jaupart and H. K. C. Perry, Laboratoire de Dynamique des Systèmes Géologiques, Institut de Physique du Globe de Paris, Tour 14-15, 4, place Jussieu, F-75252, Paris, Cedex 05, France. (perry@ipgp.jussieu.fr)

J. C. Mareschal, GEOTOP-UQAM-McGill, Université du Québec à Montréal, P.O. Box 8888, sta. "downtown," Montréal, QC, Canada H3C 3P8. (jcm@olympus.geotop.uqam.ca)

N. M. Shapiro, Laboratoire de Sismologie, Institut de Physique du Globe de Paris, Tour 14-15, 4, place Jussieu, F-75252 Paris, Cedex 05, France. (nshapiro@ipgp.jussieu.fr)